TITLE:

Effects of TiO2 crystallinity and oxygen composition on forming characteristics in Pt/TiO2/Pt resistive switching cells

AUTHOR(S):

Arahata, Masaya; Nishi, Yusuke; Kimoto, Tsunenobu

CITATION:

Arahata, Masaya ...[et al]. Effects of TiO2 crystallinity and oxygen composition on forming characteristics in Pt/TiO2/Pt resistive switching cells. AIP Advances 2018, 8: 125010.

ISSUE DATE:

2018-12-01

URL:

http://hdl.handle.net/2433/235931

RIGHT:

© 2018 Author(s). All article content, except where otherwise noted, is licensed under a Creative Commons Attribution (CC BY) license (http://creativecommons.org/licenses/by/4.0/).

京都大学学術情報リポジトリ
KURENAI 紅
Kyoto University Research Information Repository

京都大学 KYOTO UNIVERSITY
A Self-archived copy in
Kyoto University Research Information Repository
https://repository.kulib.kyoto-u.ac.jp
京都大学学術情報リポジトリ KURENAI 紅 Kyoto University Research Information Repository

AIP ADVANCES **8**, 125010 (2018)

Effects of TiO_2 crystallinity and oxygen composition on forming characteristics in Pt/TiO_2/Pt resistive switching cells

Masaya Arahata,[a] Yusuke Nishi, and Tsunenobu Kimoto
Department of Electronic Science and Engineering, Kyoto University, Kyoto 6158510, Japan

(Received 21 September 2018; accepted 3 December 2018; published online 12 December 2018)

"Forming" is a stage in resistive switching (RS) devices that occurs before switching and represents an important physical phenomenon in the universal operating mechanism of such devices. Forming in a resistance change material appears to be a kind of dielectric breakdown. In this study, we performed time-dependent forming (TDF) characterization of Pt/TiO_2/Pt resistive switching cells with TiO_2 layers of different crystallinities and oxygen compositions. We prepared two samples in which the grain boundary density and the density of oxygen vacancies differ, while both the TiO_2 layers exhibited the similar crystal structures. Our results reveal that the Weibull slope and variation of time to forming are determined by the deposition method of the Pt bottom electrode (BE) films. Moreover, the initial cell resistance and distribution of the TDF characteristics depend not only on the crystallinity but also on the oxygen composition of the TiO_2 layers. The variation of time to forming increases as the distribution of initial resistance is reduced in Pt/NiO/Pt resistive switching cells with different NiO crystallinities. Conversely, the variation of time to forming decreases as the distribution of the initial resistance is reduced in the case of the Pt/TiO_2/Pt cells. These results reflect differences in both the grain boundary density (crystallinity) and the density of oxygen vacancies (oxygen composition) of resistance change materials used in the resistive switching cells. The clear difference of crystallinities and oxygen compositions might originate from differences in the oxide deposition mode during reactive sputtering. © *2018 Author(s). All article content, except where otherwise noted, is licensed under a Creative Commons Attribution (CC BY) license (http://creativecommons.org/licenses/by/4.0/).* https://doi.org/10.1063/1.5060639

I. INTRODUCTION

In recent years, resistive random access memories (ReRAMs)[1–3] have attracted attention as a candidate for next-generation nonvolatile memory devices. ReRAM can be easily integrated with current technologies owing to its simple structure featuring a transition metal oxide (TMO) as the resistance change material sandwiched between two metallic electrodes. Various resistance change materials have been reported in binary-TMO devices, such as NiO,[4–7] TiO_2,[8–10] Ta_2O_5,[11–13] and HfO_2.[14–16] ReRAM also has attractive features, such as fast operation, low power consumption, and compatibility with complementary metal-oxide semiconductor devices. Thus, ReRAM devices are widely applied as memory resistors[17] and in neuromorphic applications. Resistive switching (RS) phenomenon in binary-TMO-based ReRAM has been intensively investigated, and a filament model is widely accepted to explain this phenomenon.[18] According to this model, forming is considered to be a stage during which a conductive filament forms by a kind of dielectric breakdown of a pristine cell under electric stress. Although forming is a crucial process for elucidating the universal mechanism of RS phenomenon, the filament model is only qualitative and it remains unclear where the conductive filament is created.

[a]arahata@semicon.kuee.kyoto-u.ac.jp

 © Author(s) 2018

京都大学 KYOTO UNIVERSITY
A Self-archived copy in
Kyoto University Research Information Repository
https://repository.kulib.kyoto-u.ac.jp
京都大学学術情報リポジトリ KURENAI 紅 Kyoto University Research Information Repository

In our previous work, we analyzed the conductive filament of a NiO thin film in a Pt/NiO/Pt cell. The results suggested that oxygen vacancy (V_O) segregation at grain boundaries in the NiO thin film is one of the main physical origins of conductive filaments,[19,20] and that distributions of the grain boundaries in resistive switching materials depend on NiO crystallinity.[21] Thus, a deposition method of the Pt bottom electrode (BE) layer not only affects the crystallinity of the Pt BE layers but also that of the NiO thin films. We confirmed that the differences in crystallinities of the bottom electrode caused differences in the electrical properties of the Pt/NiO/Pt cells, including the time-dependent forming (TDF) characteristics.[21]

Titanium dioxide (TiO_2) has been examined extensively because it has many applications, such as photocatalysts, powder pigments, antibacterial agents, as well as resistance change materials, where it shows both unipolar and bipolar RS characteristics. In addition, TiO_2 is one of the most promising switching materials of ReRAM cells because of satisfactory RS characteristics and a high compatibility with conventional production lines.[9,22,23] TiO_2 was also suggested as the material of memristors.[22] To induce RS phenomenon in TiO_2–based ReRAM cells, the formation of a conductive filament including the Vos or composed of Ti_nO_{2n-1} (Magneli phase) is required.[24] Although a few papers have reported on the electrical properties of resistive switching cells with some TiO_2 crystallinities,[24,25] it remains unclear how conductive filaments are formed at grain boundaries in a TiO_2 layer. In this study, we investigate the effects of crystallinity and oxygen composition of TiO_2 layers on the initial electrical characteristics of Pt/TiO_2/Pt resistive switching cells. We experimentally compared the effects of TiO_2 crystallinity in Pt/TiO_2/Pt cells with those in the case of Pt/NiO/Pt cells. Moreover, we discuss the difference of forming characteristics, such as the variation of time to forming t_{form} based on the observed phenomena in Pt/TiO_2/Pt and Pt/NiO/Pt cells.

II. EXPERIMENTAL PROCEDURE

Pt/TiO_2/Pt resistive switching cells were fabricated as follows. First, a Ti thin film as an adhesive and a Pt layer as a bottom electrode (BE) were deposited on a SiO_2 (200 nm)/Si substrate by either dc sputtering (SP) or electron beam (EB) evaporation. The thickness of the Pt BE layers was 25-70 nm. Next, a TiO_2 layer as a resistive switching layer was deposited on the BE layer by radio-frequency (rf) reactive sputtering in an Ar and O_2 gas mixture with the use of a metal Ti target. The Ar and O_2 gas flow rates were 10.0 and 1.0 sccm, respectively. The total pressure and substrate temperature during TiO_2 sputtering were held at 0.675 Pa and room temperature, respectively. The thickness of the TiO_2 layers was in the range of 30 to 50 nm for the resistive switching cells and over 100 nm for structural analyses. Pt films as top electrodes (TEs) with a circular shape and diameters of 100-200 μm were deposited on the TiO_2 layer by EB evaporation through a metal shadow mask. The thickness of the Pt TE films was approximately 25 nm. In the following, we refer to samples with Pt/TiO_2/Pt cells based on Pt BE films deposited by either dc sputtering or EB evaporation as "SP-Pt samples" or "EB-Pt samples", respectively.

Figure 1 shows typical atomic force microscope (AFM) images of the TiO_2 and Pt BE layers of both the SP-Pt and EB-Pt samples. The thickness of the Pt BE of the SP-Pt sample was 60 nm and that of the EB-Pt samples was either 70 or 25 nm (the latter is designated here as the thinner EB-Pt sample). The thickness of TiO_2 was approximately 30 nm. A root-mean-square (RMS) roughness value from a scan area of 0.5 μm × 0.5 μm was used as an index for the sample surface roughness. Typical roughness values are summarized in Table I. The roughness value of the Pt BE surface of the EB-Pt sample was greater than that of the SP-Pt sample. Conversely, the Pt BE roughness value of the thinner EB-Pt sample was smaller than that of the EB-Pt sample. Although the thickness of the TiO_2 layers was almost the same, the roughnesses of both the Pt BE and the TiO_2 surface increased as the thickness of the Pt BE layer became larger. Thus, the TiO_2 surface basically reflected the Pt BE surface and the different deposition methods for the Pt BE layer induced differences on the TiO_2 surface. This result is similar to our previous results that the NiO surface reflects the Pt BE surface in the Pt/NiO/Pt resistive switching cells.[21]

In all of electrical measurements, a Pt BE was grounded and the positive or negative voltage was applied to a Pt TE. Current-voltage (*I-V*) characteristics and the time to forming (t_{fom}) of Pt/TiO_2/Pt cells in the initial state were measured in a voltage sweep mode and under a constant voltage using a

京都大学 KYOTO UNIVERSITY
A Self-archived copy in
Kyoto University Research Information Repository
https://repository.kulib.kyoto-u.ac.jp
京都大学学術情報リポジトリ KURENAI 紅 Kyoto University Research Information Repository

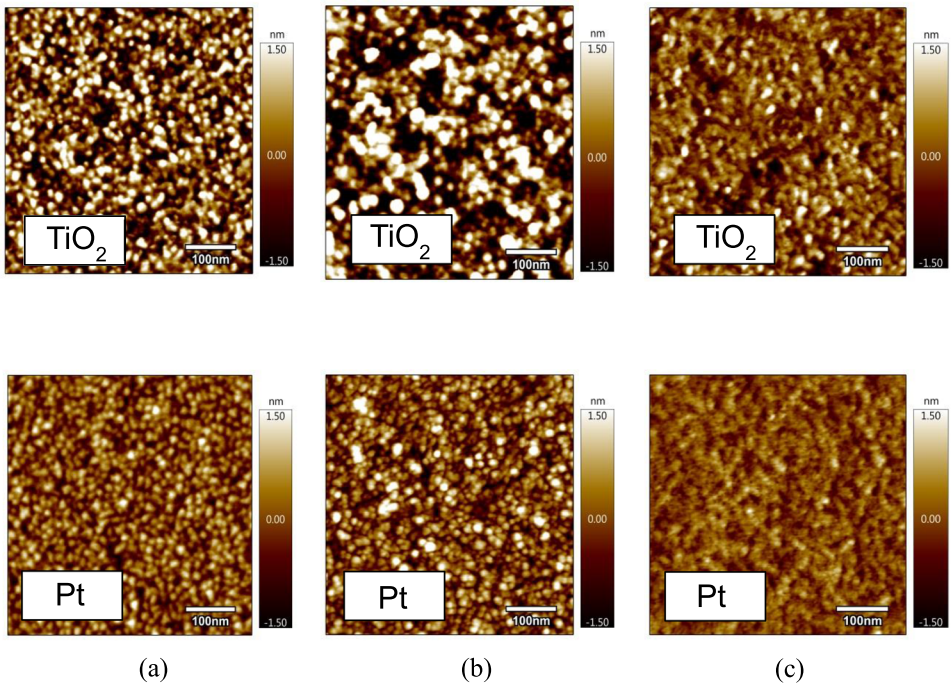

FIG. 1. AFM images of TiO_2 layers with a thickness of approximately 30 nm and Pt BE layers of the (a) SP-Pt sample and (b) the EB-Pt samples and (c) thinner EB-Pt sample. Thicknesses of the Pt BE layers are (b) 70 nm and (c) 25 nm.

TABLE I. Typical RMS roughness values of Pt BE and TiO_2 layers of SP-Pt sample, EB-Pt sample, and thinner EB-Pt sample.

RMS roughness	SP-Pt sample	EB-Pt sample	thinner EB-Pt sample
Pt BE layer	0.50 nm	0.64 nm	0.34 nm
TiO_2 layer	0.93 nm	1.32 nm	1.05 nm

Keithley 4200 semiconductor parameter analyzer at room temperature, respectively. After forming, we confirmed that almost all the cells in both samples showed repeated RS characteristics.

We measured X-ray diffraction (XRD) patterns of the SP-Pt samples and EB-Pt samples to examine the TiO_2 crystallinity. In our previous work, we confirmed that Pt BE layers deposited by sputtering preferentially orient to the [111] direction and that (111) and (200) diffraction peaks appear from the Pt BE layers deposited by EB evaporation.[21] We also confirmed differences in the crystallinity of Pt BE deposited by different methods through out-of-plane XRD measurement in the SP-Pt samples and the EB-Pt samples.[21] We performed in-plane XRD measurements, irradiating both samples with X-ray at a small incident angle because the intensities of the diffraction peaks from polycrystalline thin films in out-of-plane XRD measurements were weak. The incident angle was set to the 0.3° in this study.

III. RESULTS AND DISCUSSION

A. TiO_2 crystallinity

The in-plane XRD curves of the Pt and TiO_2 layers in the SP-Pt sample and the EB-Pt sample are shown Figure 2(a) and 2(b), respectively. Although the SP-Pt sample was expected to exhibit only a (220) diffraction peak from the Pt BE layers, corresponding to the $[1\bar{1}0]$ plane perpendicular to the [111] preferential orientation, additional diffraction peaks from (111), (200), and (311) were detected as shown in Fig. 1(a). Thus, the in-plane XRD measurements showed that the SP-Pt sample contained Pt TE layers and additional peaks derived from the polycrystalline Pt TE layers with an

京都大学 KYOTO UNIVERSITY
A Self-archived copy in
Kyoto University Research Information Repository
https://repository.kulib.kyoto-u.ac.jp
京都大学学術情報リポジトリ KURENAI 紅 Kyoto University Research Information Repository

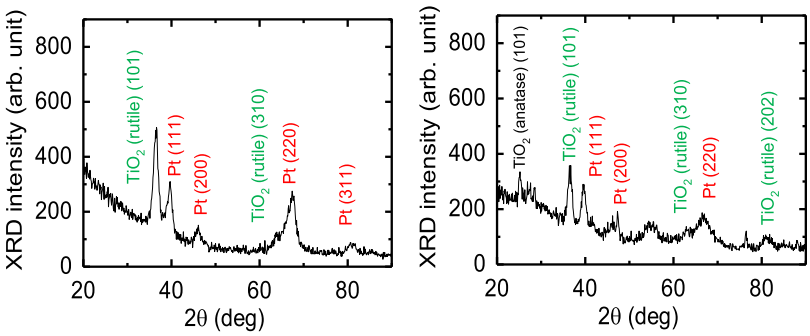

FIG. 2. X-ray diffraction curves of (a) the SP-Pt samples and (b) the EB-Pt samples. X-ray wavelength is 0.1540562 nm (Cu Kα1).

almost random orientation. Moreover, the diffraction peaks from the TiO_2 layers in both samples revealed that the crystalline structures of the TiO_2 layers in both samples were mainly rutile-type polycrystals. Here, the integrated intensity ratio of the rutile-type TiO_2 (101) to (310) diffraction peaks in the SP-Pt sample was more than twice as high as that of the EB-Pt sample. The EB-Pt sample peak ratio was very similar to that of powdered TiO_2 with randomly oriented crystallites. Moreover, we estimated the grain size from full width at half maximum (FWHM) of the rutile-type TiO2 (101) diffraction peaks by using the Scherrer equation. The FWHM is 1.0 degree in the EB-Pt sample and 1.3 degree in the SP-Pt sample. Although the estimated grain size of TiO_2 in the EB-Pt sample is a bit larger than that in the SP-Pt sample, the in-plane orientation of the rutile-type TiO_2 (101) in the SP-Pt sample was greater, and the EB-Pt sample included an anatase-type TiO_2 component, as shown in Fig. 2(b). These results indicate that the TiO_2 crystallinity of the SP-Pt sample was better than that of the EB-Pt sample. Therefore, the crystal orientation of the TiO_2 layers strongly depends on the deposition method of the lower Pt BE layers. In our previous study, we also observed that the crystallinity of NiO thin films depends on the crystallinity of Pt BE in the Pt/NiO/Pt resistive switching cells.[21]

Typical cross-sectional transmission electron microscope (TEM) images of the SP-Pt sample and EB-Pt sample with a TiO_2 thickness of more than 100 nm are shown in Figs. 3(a) and 3(b), respectively. Although the TiO_2 layers of both samples consisted of granules near the TiO_2/Pt BE interface, the crystallinity of the TiO_2 layer in the SP-Pt sample appeared to be better than that in the EB-Pt sample, particularly at the region far from the interface. Selected area electron diffraction (SAED) images taken from the area in Fig. 3(a) showed TiO_2 at a distance of approximately 60 nm from the TiO_2/Pt interface and the area in TiO_2 near the interface in the EB-Pt sample (Fig. 4). Thus, the EB-Pt sample in Fig. 4(b) exhibits more diffraction spots based on different crystalline phases than does SP-Pt sample Fig. 4(a). As a result, at greater distances from the TiO_2/Pt interface, the

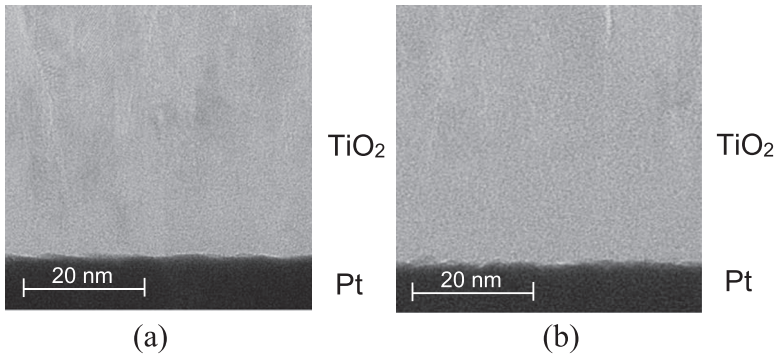

FIG. 3. Cross-sectional TEM images of (a) SP-Pt samples and (b) EB-Pt samples.

京都大学 KYOTO UNIVERSITY
A Self-archived copy in
Kyoto University Research Information Repository
https://repository.kulib.kyoto-u.ac.jp
京都大学学術情報リポジトリ KURENAI 紅 Kyoto University Research Information Repository

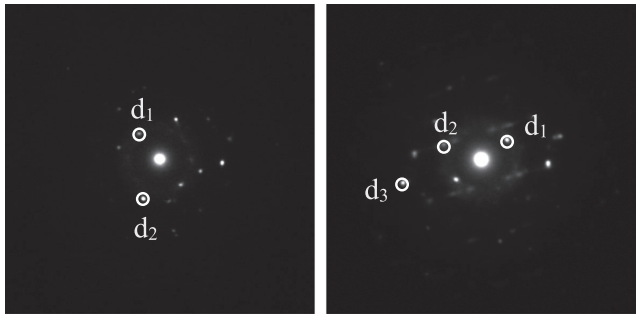

FIG. 4. Selected area electron diffraction (SAED) patterns of (a) an area of TiO_2 at a distance approximately 60 nm from the TiO_2/Pt interface and (b) an area of TiO_2 near the interface of the EB-Pt sample. Several diffraction spots of d_1, d_2, and d_3 indicates rutile-type TiO_2 (110), (101), and (310), respectively.

crystallinity of the TiO_2 layer becomes better, which suggests that the influence of crystal orientation of the Pt BE on the crystallinity of the TiO_2 layer decreased gradually during deposition. Note that the difference of the crystallinity of the TiO_2 layer along the thickness direction is not an important factor for the Pt/TiO_2/Pt resistive switching cells because the TiO_2 layers are sufficiently thin. Rather the crystallinity depends on the deposition method of the Pt BE layers as described above.

B. Initial forming characteristics

Figure 5 shows typical *I*-*V* characteristics in the initial state obtained by a voltage sweep of the Pt/TiO_2/Pt resistive switching cells in the SP-Pt sample and the EB-Pt sample with a TiO_2 thickness of 30 nm. The current compliance (I_{comp}) was set to be 10 mA to prevent catastrophic breakdown of the cells at forming. The voltage drop backs in the plot mean occurrence of forming. Although variation of forming characteristics among the cells in the same sample was large, the forming voltage of the cells based on the SP-Pt sample was clearly larger than that of the EB-Pt sample. The distributions of initial cell resistance at 1 V (R_{ini}) for the SP-Pt and EB-Pt samples with different TiO_2 thickness are shown in Fig. 6. In the case of a TiO_2 thickness of 30 nm, the ranges of R_{ini} in the SP-Pt and EB-Pt samples were 40-350 GΩ and 0.1 MΩ-2 GΩ, respectively. This result indicates that the R_{ini} values in the SP-Pt sample are greater than those in the EB-Pt sample. Furthermore, the variation of R_{ini} in the SP-Pt sample is much smaller than that in the EB-Pt sample. Conversely, the range of forming voltage (V_{form}) values in the SP-Pt sample was 5-9.3 V, whereas that in the EB-Pt sample was 2.7-5.1 V. We found similar tendencies for the forming characteristics in samples with the other TiO_2 thicknesses. As a result, the variation of V_{form} did not affect that of R_{ini} although V_{form} tended to increase with increase in R_{ini}.

We measured the time to forming (t_{form}) of the cells under a constant V_S and I_{comp} of 10 mA. Figure 7 shows the typical current-time (*I*-*t*) characteristics in the SP-Pt sample and the EB-Pt sample

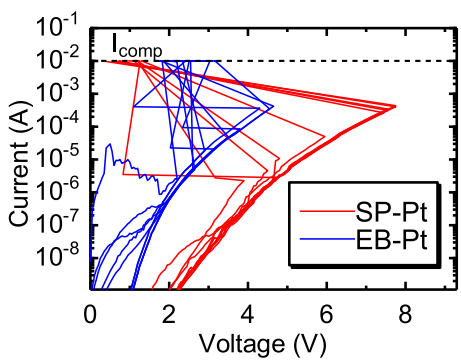

FIG. 5. Typical current-voltage curves in the SP-Pt and EB-Pt sample with a TiO_2 thickness of 30 nm.

京都大学 KYOTO UNIVERSITY
A Self-archived copy in
Kyoto University Research Information Repository
https://repository.kulib.kyoto-u.ac.jp
京都大学学術情報リポジトリ KURENAI 紅 Kyoto University Research Information Repository

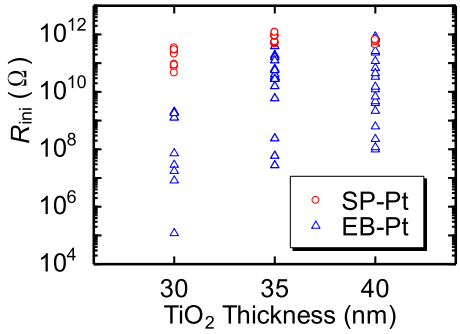

FIG. 6. TiO_2 thickness dependence of initial resistance at 1 V (R_{ini}) in the SP-Pt and EB-Pt samples.

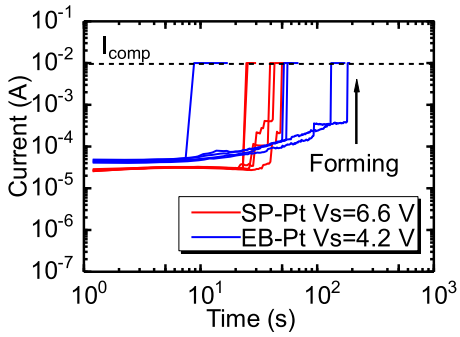

FIG. 7. Typical current-time curves of the SP-Pt and EB-Pt samples with a TiO_2 thickness of 35 nm under constant voltages of 6.6 and 4.2 V, respectively.

with a TiO_2 thickness of 35 nm under V_S = 6.6 and 4.2 V, respectively. Here, we regard t_{form} as the time to reach I_{comp} despite a gradual increase in current before forming. The range of t_{form} in the SP-Pt samples was smaller than that in the EB-Pt samples although the current levels before forming were very similar to each other. The similarity of the current levels under different values of V_S indicates that the differences in the voltage were a few tens of μA for the SP-Pt and EB-Pt samples as shown in Fig. 5. Moreover, the small range of the current level (approximately 0.01-1 mA) before forming in both samples is not linked with the initial cell resistance at voltages less than approximately 2 V (including R_{ini}), as can be seen from Fig. 5.

To obtain more insight into the variation of forming characteristics, we investigated the TDF characteristics of the Pt/TiO_2/Pt cells with various cell areas (A_{ox}). When defects, which cause dielectric breakdown or forming, are randomly distributed according to Poisson statistics in oxide thin films, the area-scaling law using the reference area A_0 can be expressed by[21,26,27]

$$W = \ln\left[-\frac{\ln(1-F)}{\frac{A_{ox}}{A_0}}\right] = \beta \ln t_{form} + \text{const.}$$

where W is the index of Weibull distribution (Weibit), F is the cumulative forming probability, and β is the shape parameter of Weibull distribution. Figures 8(a) and 8(b) show the Weibits of t_{form} under V_S of 6.6 and 6.0 V in the SP-Pt and EB-Pt samples with a TiO_2 thickness of 35 and 50 nm normalized by A_0 of π (100 μm/2)^2 applying to the area-scaling law, respectively. Although some data points with Weibits of less than -2 lay outside the lines in both samples, most data points followed the same lines with different Weibull slopes (β) irrespective of the TiO_2 thickness. These results indicate that formation of the conductive filament under a constant voltage in the TiO_2 layers follows weakest-link theory. Furthermore, we can speculate the weakest spots are randomly distributed, as described by Poisson statistics, according to the area-scaling law. From the difference between the Weibull slopes of ~2.5 in the SP-Pt sample and ~1.1 in the EB-Pt sample, the variation of t_{form} under a constant voltage in the SP-Pt sample is smaller than that in the EB-Pt sample.

京都大学 KYOTO UNIVERSITY
A Self-archived copy in
Kyoto University Research Information Repository
https://repository.kulib.kyoto-u.ac.jp
京都大学学術情報リポジトリ KURENAI 紅 Kyoto University Research Information Repository

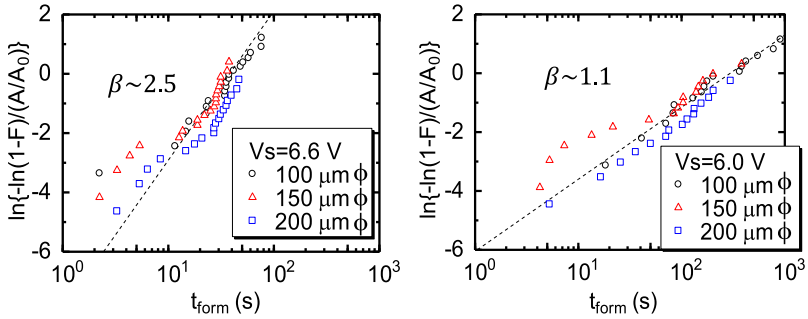

FIG. 8. Weibits of time to forming (t_{form}) normalized by cell sizes at a reference area (A_0) of π (100 μm/2)^2 in (a) the SP-Pt sample and (b) the EB-Pt sample.

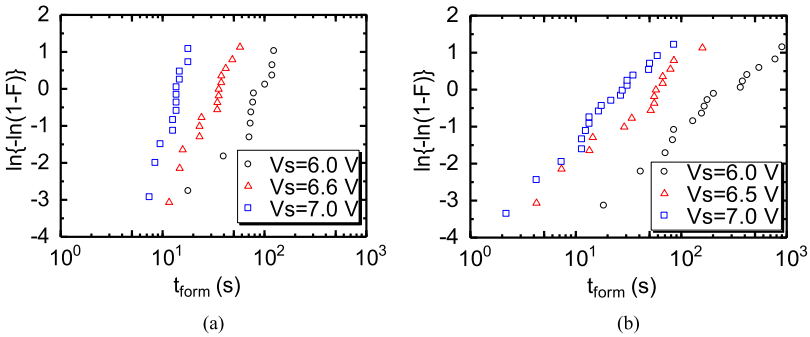

FIG. 9. Dependence of the Weibits of time to forming (t_{form}) on the applied constant voltage (V_s) in (a) the SP-Pt samples and (b) the EB-Pt samples.

The dependencies of the Weibits of t_{form} on the applied constant voltage of 6-7 V are shown in Fig. 9 (based on the same samples shown in Fig. 8). The value of t_{form} decreased as V_s increased in the both samples. Note that the β values of ~2.5 in the SP-Pt samples were almost independent of the applied voltage and these values were larger than the β of ~1.1 in the EB-Pt samples. In our previous work on Pt/NiO/Pt cells, the β value of ~0.9 in SP-Pt samples was smaller than β of approximately 1.5 in the EB-Pt samples.[21] Thus, the variation of t_{form} values in the SP-Pt samples was smaller than that in the EB-Pt samples with TiO_2 layers, which is the opposite trend to the case for NiO layers.

C. Differences in the electrical characteristics of EB-Pt and SP-Pt samples

The results of cross-sectional TEM and XRD suggest that the TiO_2 layer in both samples included granular grains of a TiO_2 crystal. We can assume that the grain boundary density in the SP-Pt samples is lower than that in the EB-Pt samples mainly because the crystallinity of the TiO_2 layer in the SP-Pt samples is better than that in the EB-Pt samples based on our in-plane XRD results. Here, we investigated the ratio of O to Ti in the TiO_2 layers in both samples by Rutherford backscattering spectrometry (RBS). The oxygen composition x in the TiO_x was 1.57 for the SP-Pt samples and 1.41 for the EB-Pt samples. Thus, TiO_2 layers in the SP-Pt samples contained fewer oxygen vacancies (V_Os) than those in the EB-Pt samples, as estimated from our previous results of V_O segregation at grain-boundary triple points in resistance change oxide layers.[20,28] Previous TEM energy-dispersive X-ray mapping images of NiO layers with various oxygen compositions, have shown that more V_O-rich (O-deficient) and Ni-rich spots appear at grain-boundary triple points as the oxygen composition decreases.[28] Another reason for more oxygen vacancies in the EB-Pt samples is that the initial resistance values before forming in the SP-Pt samples were considerably higher than those in the

京都大学 KYOTO UNIVERSITY
A Self-archived copy in
Kyoto University Research Information Repository
https://repository.kulib.kyoto-u.ac.jp
京都大学学術情報リポジトリ KURENAI 紅 Kyoto University Research Information Repository

EB-Pt sample. Note that there are considerable differences of the initial cell resistance and forming characteristics of the SP-Pt and EB-Pt samples irrespective of thickness (25-70 nm) as well as the surface roughness of Pt BE layers. Thus, the structural and electrical properties of the cells depend on the oxygen composition of the TiO_2 layers and the crystallinity of both the TiO_2 and Pt BE layers.

Next, we discuss the difference of the variation of time to forming (t_{form}) between the SP-Pt and EB-Pt samples. We can assume that conductive paths with minimum resistivity are created along grain boundaries (mainly at their triple points) with nearly random orientations in the TiO_2 layer. Furthermore, the conductive filaments likely originate from the weakest defects at forming and are created along one of the conductive paths. The multiple conductive paths naturally introduce more candidates for conductive filaments at forming and a larger variation of the forming characteristics, such as t_{form} under a constant voltage stress (Fig. 7). Fewer V_Os are distributed in the TiO_2 layer in the SP-Pt samples than in the EB-Pt samples; thus, the conductive paths are less pronounced in the SP-Pt samples than in the EB-Pt samples and the variation of t_{form} in the SP-Pt samples became smaller than that of the EB-Pt samples.

Finally, we compared the Weibull distributions of the Pt/TiO_2/Pt cells with the results of Pt/NiO/Pt cells. In the Pt/NiO/Pt cells, the Weibull slope β under a constant voltage was independent of the applied voltage and cell size, which was approximately 0.9 and 1.5 in the SP-Pt and EB-Pt samples, respectively. We explain this relationship with β based on the difference in the NiO crystallinities with columnar or granular structures in NiO layers of the Pt/NiO/Pt cells in the SP-Pt samples or the EB-Pt samples, respectively.[21] The columnar structure includes less candidates of weakest defects at forming because of fewer conductive paths along the grain boundaries than the granular structure and therefore, the variation of t_{form} in the SP-Pt samples is actually greater than that in the EB-Pt samples. Conversely, in the Pt/TiO_2/Pt cells, TiO_2 crystal structures in both samples are commonly composed of granular grains. As a result, the variation of t_{form} decreases as the distribution of R_{ini} decreases in the Pt/TiO_2/Pt cell, while the variation of t_{form} increases as the distribution of R_{ini} decreases in the Pt/NiO/Pt cells as mentioned above. This clear difference might be partly attributed to different oxide deposition modes during reactive sputtering. In the case of NiO deposition in a metallic mode, the NiO layers react on the sample surface and the NiO crystallinity is affected by the crystallinity of the Pt BE layers. Conversely, in the case of TiO_2 deposition in an oxide mode, the effect of crystallinity of the Pt BE layers on TiO_2 layers seems to be weaker because of oxide formation at the surface of a Ti sputtering target.[29] Although TiO_2 crystal structures are commonly composed of granular grains, the differences in crystal orientations and amounts of oxygen vacancies in the TiO_2 layers of the SP-Pt samples and EB-Pt samples were caused by the crystallinity of the underlying Pt BE layers, leading to the different forming characteristics.

IV. CONCLUSIONS

In conclusion, we have investigated the effect of TiO_2 crystallinity and oxygen composition on electrical characteristics in Pt/TiO_2/Pt resistive switching cells based on Pt BE layers deposited by two different methods. Although both the TiO_2 layers exhibited granular structures in the two sample types, based on Pt deposited by sputtering or EB evaporation, the density of oxygen vacancies differs in each sample. We performed time-dependent forming (TDF) measurements of the Pt/TiO_2/Pt cells. The Weibull slope of time to forming was independent of the applied constant voltage, at approximately 2.5 and 1.1 in the SP-Pt and EB-Pt samples, respectively. Furthermore, almost all the data points of the Weibull distribution normalized by cell size fell on the same line. This result reveals that the formation of a conductive filament in the TiO_2 thin film in the forming process followed weakest-link theory. Defects acted as the weakest spots and defects such as oxygen vacancies were almost randomly distributed in the TiO_2 thin films according to Poisson statistics. Moreover, the variation of time to forming decreased as the distribution of the initial resistance decreased in the two samples with TiO_2 thin films with different TiO_2 crystallinities, although the variation of time to forming increased as the distribution of the initial resistance decreased in the case of the NiO thin films. The distribution of TDF characteristics depends on both the crystallinities and oxygen composition of the TiO_2 layers because of the different deposition methods of the Pt BE layers.

京都大学 KYOTO UNIVERSITY
A Self-archived copy in
Kyoto University Research Information Repository
https://repository.kulib.kyoto-u.ac.jp
京都大学学術情報リポジトリ KURENAI 紅 Kyoto University Research Information Repository

This clear difference might originate from differences in the oxide deposition mode during reactive sputtering.

[1] R. Waser and M. Aono, Nat. Mater. **6**, 833 (2007).
[2] A. Sawa, Mater. Today **11**, 28 (2008).
[3] F. Pan, S. Gao, C. Chen, C. Song, and F. Zeng, Mater. Sci. and Eng. R: Reports **83**, 1 (2014).
[4] K. Kinoshita, T. Tamura, M. Aoki, Y. Sugiyama, and H. Tanaka, Jpn. J. Appl. Phys. Part 2: Letters **45**, 991 (2006).
[5] K. Tsunoda, K. Kinoshita, H. Noshiro, Y. Yamazaki, T. Iizuka, Y. Ito, A. Takahashi, A. Okano, Y. Sato, T. Fukano, M. Aoki, and Y. Sugiyama, Tech. Dig.- Int. Electron Devices Meet 4419060 (2007).
[6] S. Spiga, A. Lamperti, C. Wiemer, M. Perego, E. Cianci, G. Tallarida, H. L. Lu, M. Alia, F. G. Volpe, and M. Fanciulli, Microelectronic. Eng. **85**, 2414 (2008).
[7] Y. Nishi, T. Iwata, and T. Kimoto, Jpn. J. Appl. Phys. **50**, 015802 (2011).
[8] H. Schroeder and D. S. Jeong, Microelectronic. Eng. **84**, 1982 (2007).
[9] J. H. Yoon, J. H. Han, J. S. Jung, W. Jeon, G. H. Kim, S. J. Song, J. Y. Seok, K. J. Yoon, M. H. Lee, and C. S. Hwang, Adv. Mater. **25**, 1987 (2013).
[10] C. Rohde, B. J. Choi, D. S. Jeong, S. Choi, J.-S. Zhao, and C. S. Hwang, Appl. Phys. Lett. **86**, 262907 (2005).
[11] J. J. Yang, M.-X. Zhang, J. P. Strachan, F. Miao, M. D. Pickett, R. D. Kelley, G. Medeiros-Ribeiro, and R. S. Williams, Appl. Phys. Lett. **97**, 232102 (2010).
[12] W. Kim, S. Menzel, D. J. Wouters, Y. Guo, J. Robertson, B. Roesgen, R. Waser, and V. Rana, Nanoscale **8**, 17774 (2016).
[13] M. Terai, Y. Sakotsubo, S. Kotsuji, and H. Hada, IEEE Electron Device Lett. **31**, 5401057 (2010).
[14] S. Yu, H.-Y. Chen, B. Gao, J. Kang, and H.-S. P. Wong, ACS Nano **7**, 2320 (2013).
[15] S. Lee, W.-G. Kim, S.-W. Rhee, and K. Yong, J. Electrochem. Soc. **155**, 92 (2008).
[16] T. Nagata, M. Haemori, Y. Yamashita, H. Yoshikawa, Y. Iwashita, K. Kobayashi, and T. Chikyow, Appl. Phys. Lett. **99**, 223517 (2011).
[17] J. J. Yang, M. D. Pickett, X. Li, D. A. A. Ohlberg, D. R. Stewart, and R. S. Williams, Nat. Nanotechnol. **3**, 429 (2008).
[18] Q. Liu, J. Sun, H. Lv, S. Long, K. Yin, N. Wan, Y. Li, L. Sun, and M. Liu, Adv. Mater. **24**, 1844 (2008).
[19] T. Iwata, Y. Nishi, and T. Kimoto, Jpn. J. Appl. Phys. **52**, 041801 (2013).
[20] H. Sasakura, Y. Nishi, and T. Kimoto, Appl. Phys. Lett. **107**, 233510 (2015).
[21] Y. Nishi and T. Kimoto, J. Appl. Phys. **120**, 115308 (2016).
[22] D. B. Strukov, G. S. Snider, D. R. Stewart, and R. S. Williams, Nature **453**, 80 (2008).
[23] G. H. Kim, J. H. Lee, Y. Ahm, W. Jeon, S. J. Song, J. Y. Seok, J. H. Yoon, K. J. Yoon, T. J. Park, and C. S. Hwang, Adv. Funct. Mater. **23**, 1440 (2013).
[24] D.-H. Kwon, K. M. Kim, J. H. Hang, J. M. Jeon, M. H. Lee, G. H. Kim, X.-S. Li, G.-S. Park, B. Lee, S. Han, M. Kim, and C. S. Hwang, Nat. Nanotechnol. **5**, 148 (2010).
[25] H. Mahne, S. Slesazeck, S. Jakschik, I. Dirnstorfer, and T. Mikolajick, Microelectronic. Eng. **88**, 1148 (2011).
[26] E. Y. Wu and R.-P. Vollertsen, IEEE Trans. Electron Devices **49**, 2131 (2002).
[27] R. Degraeve, G. Groeseneken, R. Bellens, J. L. Ogier, M. Depas, P. J. Roussel, and H. E. Maes, IEEE Trans. Electron Devices **45**, 904 (1998).
[28] Y. Nishi, H. Sasakura, and T. Kimoto, J. Mater. Res. **32**, 2631 (2017).
[29] S. Berg and T. Nyberg, Thin Solid Films **476**, 215 (2005).